THE FLOW ON THE SURFACE OF ROTATING PROPELLER BLADE IN LOW REYNOLDS NUMBER REGION

Nobuyuki ARAI* and Katsumi HIRAOKA*
***Tokai University**

Keywords: *Wind Tunnel Testing, Propeller, Low Reynolds Number*

Abstract

The pressure distributions on the surface of the rotating propeller blade were measured directly and the flow directions on the surface of blade were also obtained by photographs of tufts. By comparing them, the flow characteristics and patterns on the surface of the rotating blade in low Reynolds region were verified.

1 Introduction

The propeller is extremely efficient propulsion mechanism in low speed region. Now, following upon the actualization of social consciousness about the environmental problem, the windmill is also developed eagerly. The optimum shape design method by Adkins-Liebeck[1], which the energy loss on the propeller disk is determined so as becoming minimum on the assumption that the wake is a constant helix flow, is used for the design method in low Reynolds number region. And the numerical calculation, for instance the wake vorticity method, is also adopted for wake prediction.

Flow on the blade, wake behind the propeller, wing tip vortices, and so on are important factors in order to determine the performance of actual propeller blade. In the design method of propeller, these flows need to be approximated with high accuracy, but there are few results that the states of flow on the blade are obtained experimentally.

In this study, following experiments of pressure measurement and tuft visualization were performed, the flow on the surface of some blades that have a wing section suited to low Reynolds number region was considered.

2 Design and manufacture of propeller blade

For the design of a propeller blade that rotates in the region of the low Reynolds number, the preceding method of optimum shape design by Adkins-Liebeck was used. In this method, an advance velocity, rotation speed of propeller, radius of blade, and a number of blades are needed. And the distributions of chord length and twist angle in spanwise direction of blade are determined by the iterating calculation to obtain the minimum values of the C_D/C_L, which is based on the distribution of circulation which the effect of the Prandtl's momentum loss function is added, corresponding Reynolds numbers at each position in the span direction. Following points were considered for the design of propeller blade for our experiment.

- A wing section that remains the high lift in the wide range of the angle of attack is adopted.
- The diameter of propeller is confined to 0.84m because the wind tunnel owned by Tokai University has 1.0- by 1.5-*m* test section area.
- In order to obtain the characteristics of propeller in low Reynolds number, Reynolds number at 80 % position in span direction is 10^5 order.

Parameters which are needed for the design are as shown in Table 1.

The shape of wing section is FX63-137 which has fine lift-drag ratio in the region that Reynolds number is 10^5.

The obtained distributions of twist angle and chord length are shown in Fig. 1. The twist

Table 1 design parameter of propeller blade.

Uniform Velocity	13 *m/s*
Rotation Speed of Propeller	550RPM
Number of blades	2
Wing Section	FX63-137
Radius of Blade	0.42*m*
Position at the Root of Blade	0.06*m*
Maximum of Chord Length	0.177*m*
Minimum o f Chord Length	0.061*m*

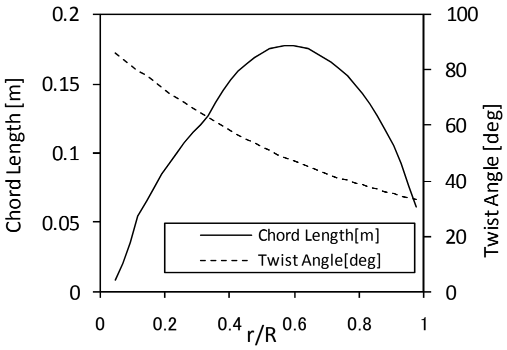

Fig. 1 Twisted Angle and Chord Length of Prop00.

angle in this figure is between the disk surface of propeller and the chord line of blade. “0-degree attached angle”, which is used in the paragraph about pressure measurement later, indicates the standard attached angle of this design value. And a measurement environment in “13*m/s* uniform velocity and 550 RPM rotation speed” is called “standard state” as the optimal condition on the design in this paper.

Fig. 2 a) shows a “Prop00” blade that was designed by the optimum shape design method. So that we compare with efficiency, pressure distribution, and flow direction by the different in the plane shape of blade, the other 3 types of blade which differ in the plane shape but have the same solidity and twist angle as the Prop00 blade were made to find the characteristics of thrust, torque, pressure distribution, and flow on the blade by the extreme differences in the planform of blade. These blades are called “Prop01”, “Prop02”, and “Prop03” in this paper. As shown in Figs. 2 b), c), and d), the Prop01, Prop02, and Prop03 blade have rectangle, trapezoid growing larger linearly toward the tip of blade, and inverse trapezoid tapering off linearly toward the tip of blade as the plane shape, respectively. These blades were made of balsa wood. And these were coated with a resin and polished over the whole surface in order to hold down the roughness of the surface.

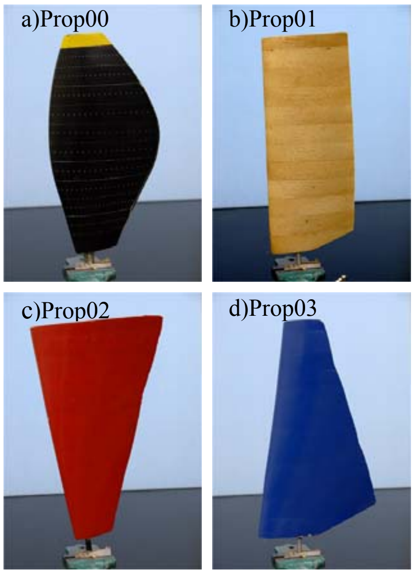

Fig. 2 4 Types of Propeller Blade.

3 Experiment device

3.1 Wind tunnel

In this experiment, a low-speed wind tunnel testing device owned by Tokai University was used. And the 6-forces balance device in the test section was employed for thrust measurement of propeller.

3.2 Driving part

As shown in Fig. 3, a driving part consists of a motor, slip ring device, and torquemeter, which each axis is connected on the rotation axis of propeller. The driving part was set on the main strut of 6-forces balance, and all

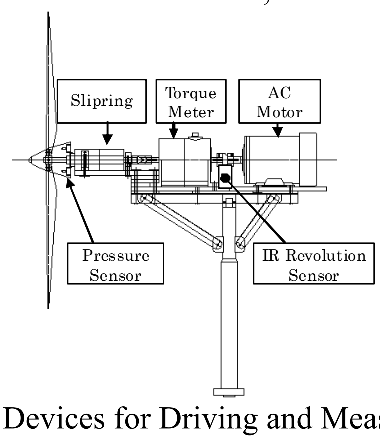

Fig. 3 Devices for Driving and Measuring.

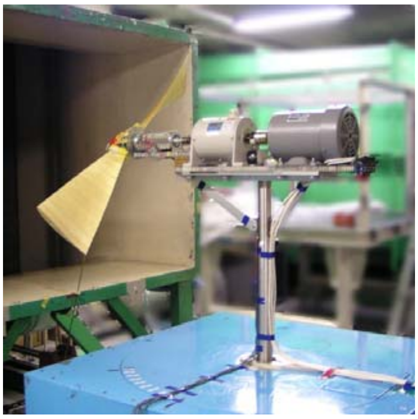

Fig. 4 Scene of Testing in Wind Tunnel.

experiments were performed under the environment that propeller rotates in the test section of wind tunnel as shown in Fig. 4.

The rotation of propeller was controlled by exclusive inverter, but the rotation speed was verified by the universal counter which indicates the frequency of electrical oscillations from the photodiode which receives the infrared reflected by the white-black pattern on the axis.

4. The pressure measurement on the surface of blade

4.1 The holes for pressure measurement on the blade

In order to measure the static pressure distribution on the surface of blade, particular blades were manufactured. As shown in Fig. 5, the small holes with 1mm diameter are arrayed on the surface. The number of holes is 319, which is 29 rows in the span direction and 11 columns in the chord direction, on one side. And a blade for measuring on the camber surface and another blade for measuring on the thrust surface were prepared. The holes are not able to be drilled in the outer area than 80% chord position at the trailing edge because the area does not have enough thickness to remain its structure with holes.

Since there are 4 pressure sensors in the nose cone, the number of holes that are able to measure at once is only 4 points. In measuring the pressure, the pressure on the surface of blade circulates to the pressure sensor in the nose cone by connecting between one hole on the blade,

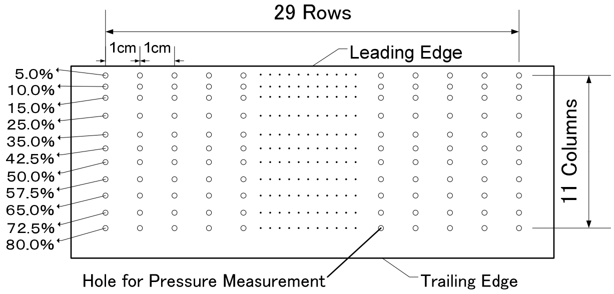

Fig. 5 Blade with Holes for Pressure Measurement.

which an aluminum tube is inserted, and one sensor with silicone tube. These aluminum tubes are needed to replace to other holes by hands every 4 holes. Furthermore, the other holes excepting for the measured 4 holes are filled in with the solid columnar fragments in order to avoid to leak into the back side.

4.2 The method of pressure measurement

The pressure measurement was performed in the condition of rotating propeller. In the nose cone under the rotating system, pressure sensors are contained. The data of pressure which is converted by sensor on the blade is recorded by PC through slip ring and A/D conversion.

The range of measurable pressure of this sensor is ±0.25 *kPa*. The data of pressure was recorded for 2.5 sec by 10 kHz sampling frequency. The recorded data of voltage was averaged at each measurement point and converted into the pressure value by a calibration data. And obtained gauge pressure was carried out the following correction for centrifugal force.

4.3 The correction for centrifugal force

Variations of pressure on the blade reach at the pressure sensor by passing through the silicon tube. In this process, the suction pressure due to the centrifugal force is also sensed by the pressure sensor because the force acts on the air in the silicon tube in rotating. Then, in order to remove the extra suction pressure from the measured pressure, a correction formula must be considered.

In the tube that keeps rotating with angular velocity ω *rad/s*, the true pressure P_e *Pa* acts at the outer end of tube where is r_e *m* position from

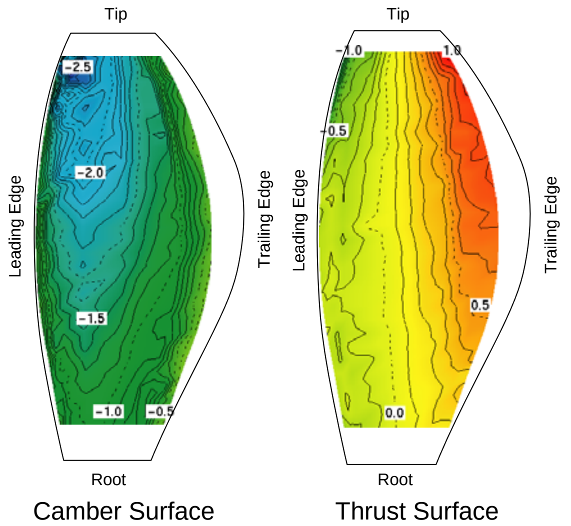

Fig. 6 Distribution of Pressure Coefficient of Prop00 (standard state).

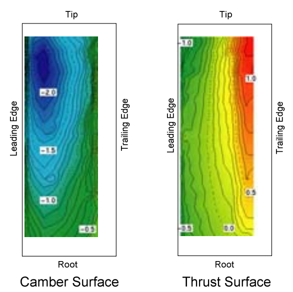

a) Prop01

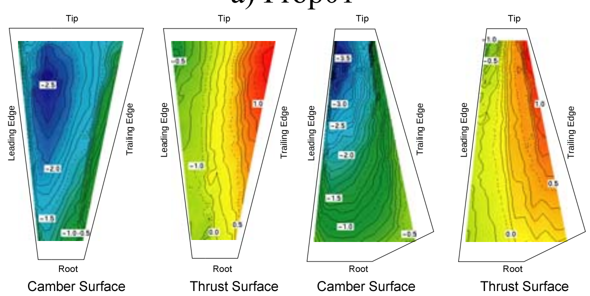

b) Prop02 c) Prop03

Fig. 7 Distribution of Pressure Coefficient of the Other Blades (standard state).

the center, and the pressure P_c *Pa* at the center of rotation, which centrifugal force doesn't influence. Supposing that the pressure P_m *Pa* was measured by the sensor that is at r_m *m* position from the center, the true pressure P_e *Pa* is represented as

$$P_e = P_m \cdot e^{\frac{\omega^2}{2RT}(r_e{}^2 - r_m{}^2)} + P_c \cdot e^{\frac{\omega^2}{2RT} r_e{}^2}, \qquad (1)$$

where temperature and gas constant for air are T *K* and R m^2/s^2K.

4.4 The distribution of pressure coefficient

Fig. 6 shows the distributions of pressure coefficient on the surface of camber side and thrust side of rotating Prop00 blade with standard state. The attached angle is 0 degree of the optimum angle. The area of blade shown in figure is limited to the area that is possible to measure, as mentioned above. The distributions of the other blades with the exception of Prop00 are shown in Fig. 7.

As shown by the distribution of Prop00 in Fig. 6, on the camber side, the tendency that the variation of suction pressure becomes larger as the outer position in spanwise direction was obtained. And, in the area where the density of contour lines changes locally near the trailing edge, especially at the tip side, a variation of pressure indicates the characteristics of a short bubble in low Reynolds number region, which the separation and reattachment of the flow occur in a relatively wide extent behind the suction peak[2]. The flow must be separated in front of the area that intervals of contour lines widen, and the flow must reattach to the surface behind the area that contour lines gather. The minimum value of pressure coefficient on the camber side is -2.73. On the other hand, on the thrust side, the pressure tends to vary equally among chord line toward the tip of blade.

The distribution of pressure coefficient of the rectangle blade Prop01 has the same tendencies with Prop00 as shown in Fig. 7 a). The minimum pressure coefficient on the camber side was -2.19 under the standard state. The characteristic distribution of contour lines, which is indicative of the presence of separation bubble, appeared on the Prop01 at the trailing edge near the tip side. The length of this disturbance in the span direction is extended a little in comparison with the area of Prop00.

Figs. 7 b) and c) show the distributions of pressure coefficient on Prop02 and Prop03 blades. The minimum pressure coefficient on the camber side of Prop02 and Prop03 were -2.52 and -3.48 under the standard state, respectively. Also on these two blades, the disturbance of density of contour lines appeared near the trailing edge. Especially, this area

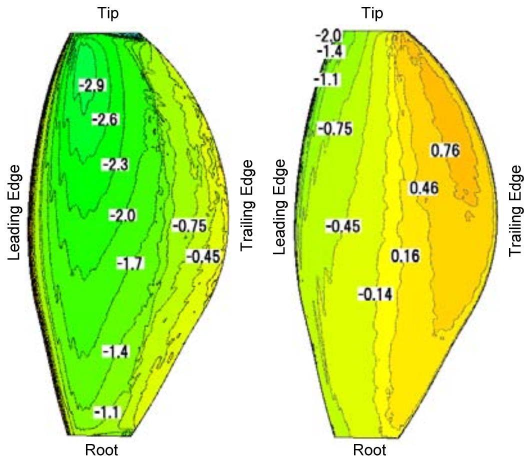

Camber Surface Thrust Surface

Fig. 8 Distribution of Pressure Coefficient on the Prop00 Blade by FLUENT.

covered over the trailing edge on Prop02 blade, and extended to the tip on Prop03 blade.

And, Fig. 8 shows the distribution of pressure coefficient on the Prop00 blade by CFD software FLUENT. Since this distribution represented the same tendency as the experimental result, both results are able to be recognized as appropriate each other.

5. Visualization of the flow on the blade surface by tuft method

5.1 Tuft and photographing

The experiment by the method of taping tuft on the surface was performed in order to visualize the direction of flow on the surface of blade. The observation by oil flow method is also considered for the visualization of the flow on the surface. But, for this experiment, the tuft method was adopted because of an environment around the test section of our wind tunnel device. The tuft was made of no-twisted embroidery floss for turning the flow direction faithfully and reducing the influence of the centrifugal force on itself.

In order to take the still photograph of tufts on the rotating blade at any circumferential position, the strobe was used with changing in the frequency of flashing as an option.

Since the strobe is set to emit the light in about 0.65 seconds, the blade that rotates with 550 *RPM* is lit by the flashlight every sixth revolutions. So, by darkening the surroundings, the blade is able to be taken a photograph for 1 second exposing.

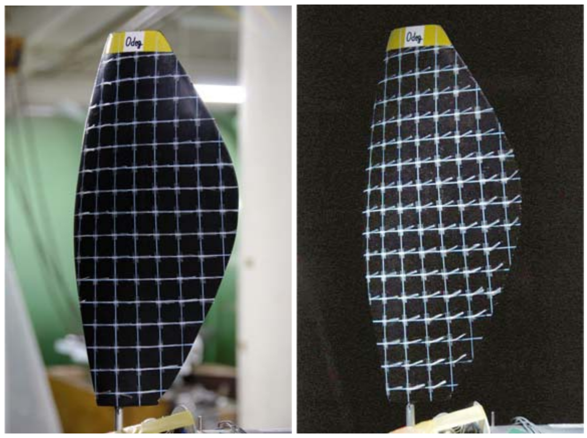

a) At Rest b)In Rotating

Fig. 9 Grid and Tuft on the Prop00 Blade.

Portions of the blade with tufts do not face with the camera because the blade is twisted. So, in order to find the direction of tuft correctly, it is necessary to consider a distortion of the surface at each point where tuft was put on. As shown in Fig. 9 a), with grid lines that was drawn on the blade, the degree of distortion for camera is able to be obtained at each point on the surface.

5.2 Estimation method for tuft experiment

By the photograph as shown in Fig. 9 b), the distribution of the bending angle of tuft, which the influence of distortion on the surface is reduced, is shown in Figs. 10 and 11. Short line shows the direction of the tuft, and a numeral in the circle shows the degree between tuft and chord line at the position.

In these results, on both sides, the characteristic of the bending angle of tuft changes at about 75% position in the radial direction. On the root side of this border on the camber surface, tufts of the trailing edge are bent more toward the tip side in comparison with tufts of the leading edge. Inversely, on the tip side of this border, some of tufts turn in chord direction near the trailing edge. Also on the thrust side, adverse tendencies appeared.

However, these bending angles of tuft shown in this figure include the deviations by the influence that centrifugal force that acts on tuft and the estimation for the angle of the tuft

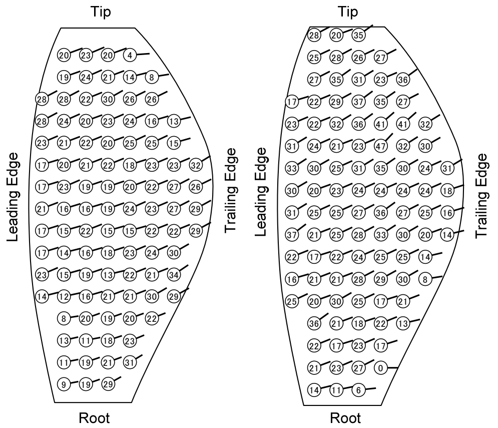

Camber Surface Thrust Surface

Fig. 10 Direction Pointed by Tuft on Prop00.

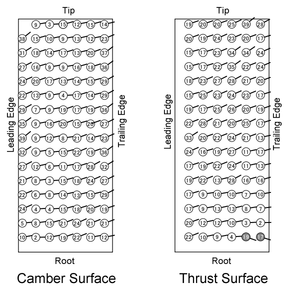

a) Prop01

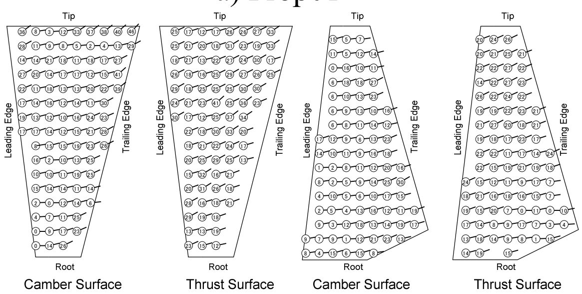

b) Prop02 c) Prop03

Fig. 11 Direction Pointed by Tuft on the Other Blade.

bent with only flow is complicated. The consideration to reduce the influence of centrifugal force is as follows.

In order to distinguish cross flows between toward tip side and root side, two kinds of behavior of tuft influenced by centrifugal force and flow were tested. When only centrifugal force influences on the tuft, the tuft is bent the most toward tip side. If the tuft on the actual blade bends outer than this tuft, the existence of cross flow toward outside must be found.

On the other hand, the actual tuft on the blade, which is influenced by the both of centrifugal force and resultant velocity, bends toward tip side with the angle between direction

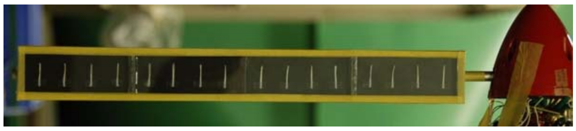

a) At Rest

b) In Rotating

Fig. 12 Bending Of Tuft With Only Centrifugal Force.

of chord and of the tuft bent with only centrifugal force. If the tuft on the actual blade bends inner than this tuft, the existence of cross flow toward inside must be found.

First, in order to measure the tendency of tuft bent with the only centrifugal force, tufts were taped on a flat plate that is packed in a case firmly closed as shown in Fig. 12. The material of tuft and the method of fixing for tuft are the same as the experiment by propeller blade. By rotating this case like propeller blade, the tufts bent with the only centrifugal force were able to be taken a photograph. The method and conditions are the same as the tuft experiment of the propeller blade.

The result is represented by a straight line in Fig. 13. By approximating the distribution of obtained angles linearly, a proportional relation as shown in this figure was obtained between the distance from the rotation center and the bending angle of tuft with centrifugal force. If the tuft on the blade turns outer than an angle that this proportional relation indicates at the same position from the center of rotation, it is clear that the force by flow acts on the tuft stronger than the centrifugal force toward the tip side of blade.

Next, in order to measure an interaction between the centrifugal force and the resultant velocity of advance velocity and circumferential velocity at the each radial position of blade, another rotating test object was taken a photograph as the same as above-mentioned experiment. As shown in Fig. 14, this test object consists of the bar of blade and the small-sized flat plate with tuft, which is the same material as the experiment of blade. This tuft is exposed to an outside so that the flow of air influence

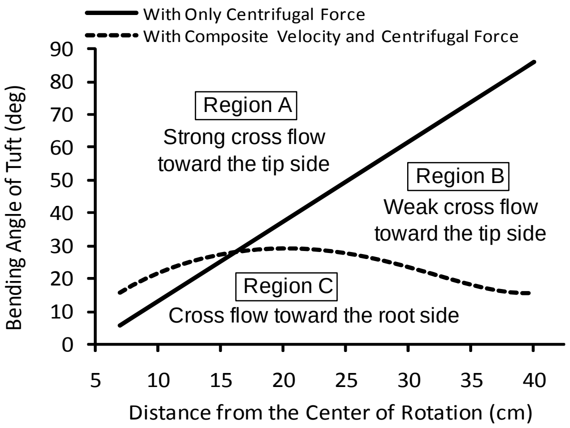

Fig. 13 Difference in Direction of Cross Flow.

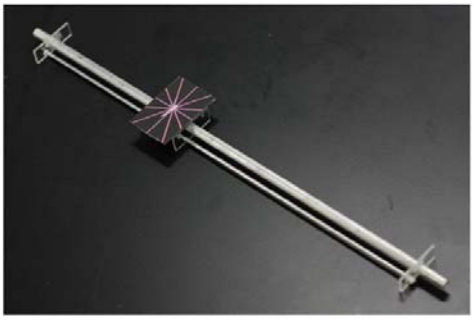

Fig. 14 Small-sized Flat Plate with Tuft.

on it. And, since an angle that the air comes in a wing element differs at each radial position on the actual propeller blade, an attached angle of the small-size flat plate was set to the same as inflow angle of the air at each radial position.

The distribution of bending angle of tuft by this experiment is also shown as chain curved line in Fig. 13. Since the bending angle of tuft changed slightly every rotation, the curved line was obtained by the polynomial approximation for the average of obtained angles at each radial position. This result indicates that the resultant velocity puts the tuft bent with centrifugal force back in the chord direction. If a tuft bent more toward the tip side than an angle that this curved line indicates on actual blade, it is clear that the resultant velocity on the blade directs more toward the root side than the chord direction, then the cross flow should occur toward the center of rotating.

The no-twisted embroidery floss has a characteristic, especially in this experiment, that the centrifugal force influences strongly on it as far as about 20 *cm* radial position, but the influence of resultant velocity is more intense than the centrifugal force on the outer side.

5.3 Actual flow direction by tuft experiments

We considered qualitatively actual directions of flow on the blade by using the results of preparatory experiments for any purpose aforesaid.

As region A in Fig. 13, the state that the tuft on the blade is bent more to the tip side than the bending angle of tuft with only centrifugal force represents that the cross flow occurs toward the tip side in the span direction. On the other hand, as region C, the state that the tuft on the blade is bent more to the root side than the bending angle of tuft with centrifugal force and resultant velocity represents that cross flow occurs toward the root side. The cross flow toward the tip side is also represented as region B, but this flow is weak in comparison with one in region A. So, each cross flow is distinguished by their strengths.

First, the strong cross flow toward the tip side is isolated. Fig. 15 shows the distribution of a remainder that the bending angle of tuft with only centrifugal force in Fig. 13 was subtracted from the bending angle of tuft at the same radial position on each blade in Figs. 10 and 11. If the remainder is positive value, it is indicative of a tendency of the cross flow toward outside. In short, the gray area indicates region A in Fig. 13.

As shown in Fig. 15 a), on the camber surface of Prop00 blade, the cross flow toward outside occurred around the root of Prop00 blade, and the area extends to trailing edge. By contrast, on the thrust surface, the cross flow toward the tip side appeared around the root side of leading edge. And there was no cross flow toward the tip side around the tip of blade. The same tendency appeared on the other three blades as shown Figs. 15 b), c), and d).

Next, the cross flow toward the root side is isolated. The distribution of a remainder that the bending angle of tuft with centrifugal force and resultant velocity in Fig. 13 was subtracted from the bending angle of tuft on each blade in Figs. 10 and 11 at the same radial position is shown in Fig. 16. If the remainder is negative value, it is indicative of a tendency of the cross flow

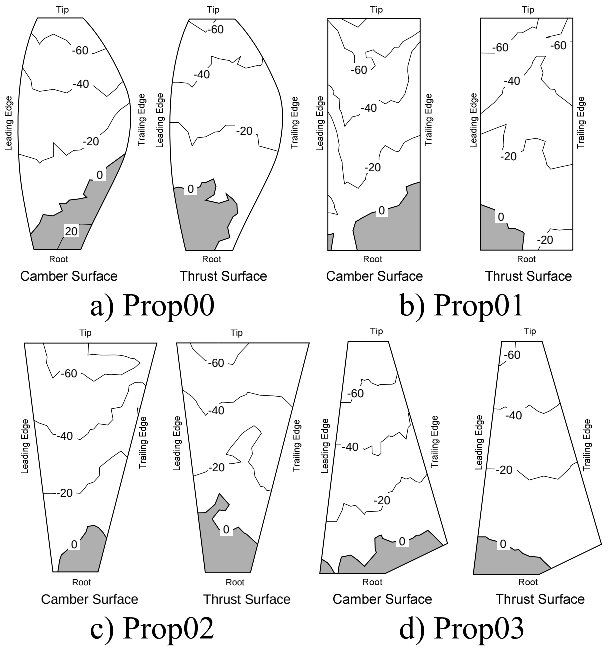

Fig. 15 Area of Cross Flow toward the tip side.

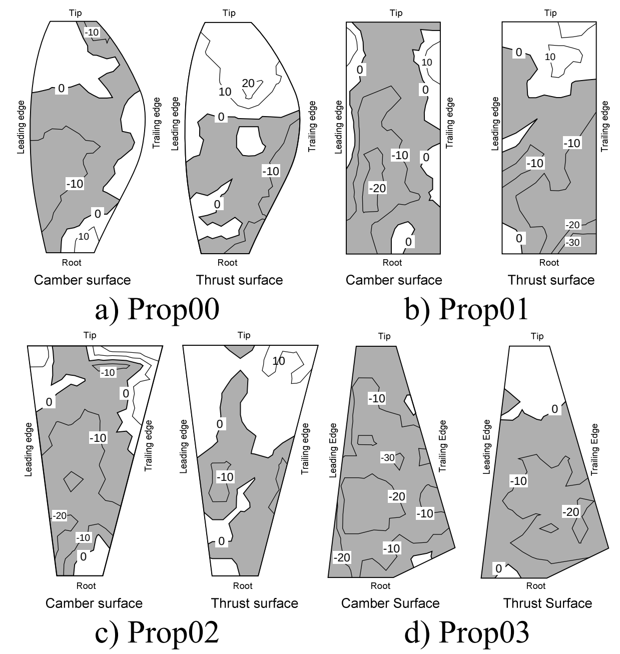

Fig. 16 Area of Cross Flow toward the root side.

toward the tip side. In brief, the gray area indicates region C in Fig. 13.

As shown in Fig. 16 a), for Prop00 blade, the gray area, where the cross flow occurred toward the root side, covered over most of surface of blade on the camber surface, and the inner than about 75% radial position on the thrust surface. Prop 01 and 02 have the same tendency as Prop00 with the exception of Prop03 that the cross flow toward inside occurred the whole camber surface.

Finally, the remainder area without region A or C is region B. For instance, these are around the leading edge near the tip on the camber surface of Prop00, the outer area than about 75% radial position on the thrust surface on each blade, and so on.

A typical flow obtained with these results was shown as a schematic depiction of flow direction on the Prop00 blade in Fig. 17. On the camber surface, the streamline drew a curve just like gathering around middle radial position of the trailing edge. But, in contrast to this, on the thrust surface, the streamline drew a curve like spreading to both sides of tip and root of the blade. The pattern of flow around the tip of the blade is similar to of the flow on the finite wing that the cross flow occurs toward the root side of wing on the upper surface and toward the tip side of wing on the lower surface near the wing tip because of generation of wing tip vortices[3]. The flow on the outer side than about 75% radial position of Prop00 blade also has the same tendency as this. In contrast, in the inner area than about 75% radial position on the camber surface, the cross flow occurred toward the tip side around the trailing edge. As a mechanism that the cross flow occurs on the sweepback wing, an increase in the strength of suction pressure toward the tip side on the blade should cause this flow toward outside.

By the analogy among the distributions in Figs. 15 and 16, it is clear that the flow on the other blades has the same tendency as Fig. 17. And, when the blade rotates, a characteristic that the streamlines draws an arc but not straight line on the frame of blade should be considered.

And, Fig. 18 shows the distribution of flow direction on the Prop00 blade by CFD software FLUENT. Since the tendencies of cross flow was the same as the experimental result, both results are able to be recognized as appropriate each other.

5.4 The mutual relation between the distribution of pressure coefficient and the direction of tuft

By comparing the occurrence distributions for cross flow in Figs. 15 and 16 with the distributions of pressure coefficient in Figs. 6

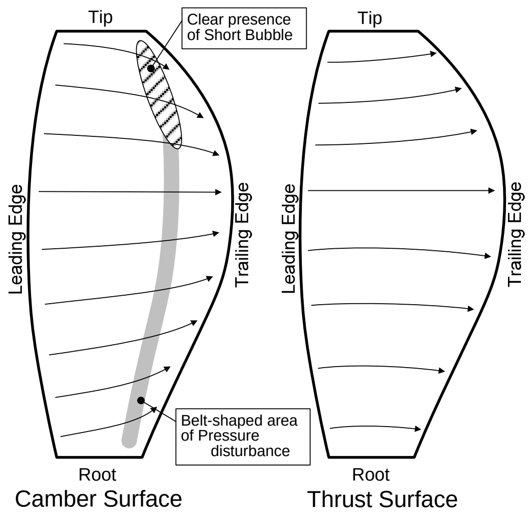

Fig. 17 Schematic diagram of Streamline on Prop00 Blade.

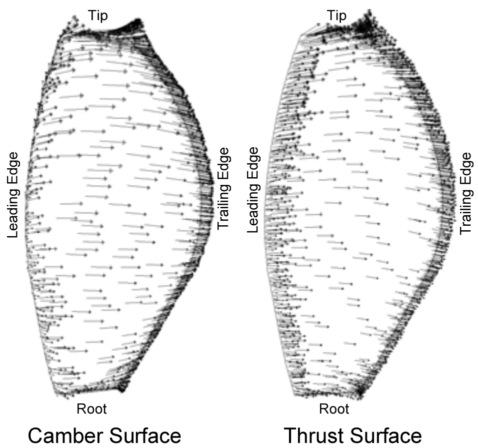

Fig. 18 Distribution of Flow Direction on the Prop00 Blade by FLUENT.

and 7 on each blade at standard state, the changes of the direction of cross flow component and the pressure distribution have features in common to each other.

On the camber surface, as shown in Figs. 6 and 7, a belt-shaped area where contour lines gather extends along the length of the leading edge on each blade. And, as shown in Fig. 16, the border line between regions C and B also distributes along the trailing edge at the same portion as the belt-shaped area. In fact, another state that the influence of the centrifugal force becomes large with the decrease in the velocity of flow also fits in region B. Also with this state, tuft is bent toward the tip side of blade. So, the flow direction did not change, instead, the velocity of flow probably decreased behind the reattachment in region B at trailing edge.

In the distribution of pressure coefficient on the camber surface of Prop00 shown in Fig. 6, as above-mentioned, a presence of short bubble was discernible clearly in an area that intervals of contour lines widen and narrow locally near the tip of trailing edge of blade. In this area, the direction of cross flow changes to the root side from the tip side between regions B and C, as shown in Fig. 16 a).

On the other hand, on the thrust surface, the contour line for pressure runs parallel to each other in the spanwise direction, and the pressure increases monotonically toward the trailing edge. The direction of flow was changed its direction toward the tip side or root side by being forced from high-pressure area near the trailing edge, as shown in Fig. 17.

And the separated flow with reattachment behind the suction peak disappears and contour lines distribute at regular interval at the just tip on the camber surface of blade. This shows the flow was avoided separating because the air that curls from the thrust surface flows in the tip on the camber surface. The same phenomenon appears on the other blade. For Prop01 and 03 blades, since the flow bent toward inside at the tip on the camber surface and outside on the thrust surface, the generation of wing-tip vortex was confirmed. And for Prop02 blade, the pressure of wide area near the tip of blade get smoothing as shown in Fig. 7 b), larger wing-tip vortex should be generated in comparison with the other blade. This inference is confirmed by a result that tufts in the second row from the tip are bent strongly toward the root side on the camber surface of blade as shown in Fig. 16 c).

6. Conclusion

At the viewpoint by comparing among each blade, the highest thrust is obtained by, in order, Prop02 which has the longest chord length on its tip, rectangle blade Prop01, optimum shape blade Prop00, and Prop03 which has the shortest chord length on the tip. On the other hand, in a similar to the result of thrust, torque becomes larger as attached angle increases. By comparing among each blade, it’s clear that the highest torque is obtained by, in order, Prop02, Prop01, Prop03, and Prop00. In comparison among the efficiencies of each blade, the most efficient blade is, in order, Prop00, which is the optimum shape blade, Prop03, Prop01, and Prop02. But the efficiencies of Prop01 and 02 became reversed in different attached angle. More the area is spread toward tip, thrust and torque are higher.

In the distribution of pressure coefficient, the separation occurred behind the region that the degree of suction pressure is high. However, around the tip, the separation disappears by the influence of tip vortex. As the area of disappearance of separation is wider, the tip vortex is stronger, so the induced drag of prop02 should be the highest.

Two propellers, prop00 and 03, that the efficiency is better than the other have the peak of the chord length away from the tip of blade. At there, the degree of the separation is weak, because the position in span direction is closer to root, suction peak is lower.

Therefore, the planform of blade that has the long chord length at the span position near the root is reasonable shape.

By the direct pressure measurement on the surface of blade, the appearance of the area where the pressure varies locally near the trailing edge was ensured. Especially, at the trailing edge on the tip side, the variation has the characteristic of separation and reattachment. And, by visualization experiment with the tuft, the flow direction on the blade was evaluated. On the camber side, the flow was bent to the root side near the tip and to the tip side near the root. In contrast, on the thrust side, the cross flow has the inverse tendency.

As mentioned above, in low Reynolds number field, the flow on the surface of blades which have the different plane shape including the optimum shape was able to be obtained by the direct pressure measurement and the tuft experiment. And new knowledge in evaluating for difference in the plane shape of blade was found.

References

[1] Adkins, C. N.and Leibeck, R. H., Design of optimum propellers, *AIAA Paper-83-0190*, 1983.

[2] Ichiro Tani, Low-speed flows involving bubble separations, *Progress in Aeronautical Science*, 5, Pergamon Press, pp.70-103, 1964.

[3] John D. Anderson, Jr., *Fundamentals of aerodynamics*, 2nd edition, McGraw-Hill, pp.315-317, 1991.

Copyright Statement